Journal of Neuroscience Research 85:285–293 (2007)

Charged Amino Acid Motifs Flanking Each Extreme of the αM4 Transmembrane Domain Are Involved in Assembly and Cell-Surface Targeting of the Muscle Nicotinic Acetylcholine Receptor

A.M. Roccamo and F.J. Barrantes*

Instituto de Investigaciones Bioquimicas and UNESCO Chair of Biophysics and Molecular Neurobiology, Bahía Blanca, Argentina

The αM4 transmembrane domain of the nicotinic acetylcholine receptor (AChR) is flanked by two basic amino acids (His^{408} and Arg^{429}) located at its cytoplasmic- and extracellular-facing extremes, respectively, at the level of the phospholipid polar head regions of the postsynaptic membrane. A series of single and double αM4 mutants (His^{408}Ala, Arg^{429}Ala, Arg^{429}Glu, His^{408}Ala/Arg^{429}Ala, and His^{408}Ala/Arg^{429}Glu) of the adult muscle-type AChR were produced and coexpressed with wild-type β, δ, and ε subunits as stable clones in a mammalian heterologous expression system (CHO-K1 cells). The mutants were studied by α-bungarotoxin ([^{125}I]α-BTX) binding, fluorescence microscopy, and equilibrium sucrose gradient centrifugation. Cell-surface [^{125}I]α-BTX binding diminished ~40% in His^{408}Ala and as much as 95% in the Arg^{429}Ala mutant. Reversing the amino acid charge (e.g., Arg^{429}Glu) abolished cell-surface expression of AChR. Fluorescence microscopy disclosed that AChR was retained at the endoplasmic reticulum, with an enhanced occurrence of unassembled AChR species in the mutant clones. Centrifugation analysis confirmed the lack of fully assembled AChR pentamers in all mutants with the exception of His^{408}Ala. We conclude that His^{408} and Arg^{429} in αM4 are involved in assembly and cell-surface targeting of muscle AChR. Arg^{429} plays a more decisive role in these two processes, suggesting an asymmetric weight of the charged motifs at each extreme of the α subunit M4 transmembrane segment.

Key words: acetylcholine receptor; plasma membrane; endoplasmic reticulum; transmembrane segments; cell-surface expression

The nicotinic acetylcholine receptor (AChR) is an ~290-kDa glycoprotein formed by five homologous, membrane-spanning subunits (for review see Karlin, 2002) with a stoichiometry of $\alpha_2\beta\gamma\delta$ (*Torpedo* electromotor synapse and fetal muscle) or $\alpha_2\beta\varepsilon\delta$ (adult muscle). The five subunits are organized around a pseudo-fivefold axis that delineates a cation-selective pathway across the membrane (Barrantes, 2003). Subunit assembly is known to occur in the endoplasmic reticulum (ER; Smith et al., 1987). Newly synthesized AChR polypeptides encounter the lumenal face of the ER, where chaperone proteins are located. The latter facilitate the rather inefficient folding and assembly reactions preceding export from the ER (Merlie and Lindstrom, 1983).

In one of the postulated mechanisms, assembly proceeds by stepwise interdependent folding and subsequent oligomerization of AChR subunits, followed by formation of αδ and αγ heterodimers (Blount and Merlie, 1990). The heterodimers undergo a series of folding events and interact with a β subunit and with each other to form a pentamer that leaves the ER and travels along the secretory pathway to the cell surface (Gu et al., 1991; Kreienkamp et al., 1995; Wanamaker et al., 2003). Those AChR proteins that do not assemble properly are retained in the ER and degraded to ensure that only physiologically active oligomers with the correct stoichiometry are transported to the cell surface.

Charged amino acid residues have been specifically implicated in the topology and mode of assembly of polytopic membrane proteins (von Heijne, 1989). The participation of the transmembrane (TM) domains of such membrane proteins has been singled out in various studies on the folding, maturation, and oligomerization steps of newly synthesized membrane-spanning proteins

Contract grant sponsor: Universidad Nacional del Sur; Contract grant sponsor: Consejo Nacional de Investigaciones Científicas y Técnicas; Contract grant sponsor: Agencia Nacional de Promoción Científica (FONCYT; to F.J.B).

*Correspondence to: F.J. Barrantes, INIBIBB, C.C. 857, B8000FWB Bahía Blanca, Argentina. E-mail: rtfjb1@criba.edu.ar

Received 25 July 2006; Revised 19 September 2006; Accepted 25 September 2006

Published online 27 November 2006 in Wiley InterScience (www.interscience.wiley.com). DOI: 10.1002/jnr.21123

at the ER (for review see von Heijne and Gavel, 1988; Schülein, 2004). In addition, the signals involved in the ER retention of misfolded AChR protein are beginning to be identified (for review see Wanamaker et al., 2003). Several studies have highlighted the importance of individual amino acids, amino acid motifs, and larger subunit domains in the trafficking and assembly of AChRs. Positively charged residues are prominently located at both ends of the M1, M3, and M4 TM regions in all AChR subunits (Blanton and Cohen, 1992). The αM4 TM region is flanked by two positively charged amino acids, Arg^{429} and His^{408}, both located at a shallow position in the membrane, at the level of the phospholipid head groups, at each extreme of the αM4 segment. A series of single- and double-mutant constructs of these motifs was produced in the adult muscle-type AChR and coexpressed with wild-type β, δ, and ε subunits. A combination of techniques is used to explore the contribution of His^{408} and Arg^{429} to receptor assembly and trafficking to the cell surface.

MATERIALS AND METHODS

Materials

[^{125}I]α-BTX (120 μCi/μmol) was from New England Nuclear (Boston, MA). Native α-bungarotoxin (α-BTX) and carbamoylcholine (Carb) were from Sigma Chemical Co. (St. Louis, MO). Alexa Fluor 488-conjugated α-BTX (Alexa Fluor 488-α-BTX), Alexa Fluor 594-α-BTX, and goat anti-rabbit and goat-anti mouse IgG antibodies labeled with Alexa Fluor 488 or Alexa Fluor 546 were all from Molecular Probes (Eugene, OR). Rabbit anticalnexin polyclonal antibody was from Stressgen Biotechnologies (Victoria, British Columbia, Canada).

Construction of AChR α1M4 cDNA Mutants

Mouse AChR cDNAs were subcloned into the SV40-based mammalian expression vector pSM. Mutations of α1M4 were obtained by bridging restriction site segments from pSMα and a synthetic double-stranded oligonucleotide mutant. The His^{408} AChR mutant was introduced by joining a 60-bp oligonucleotide from a BspMI to a Spe I site. The Arg^{429} mutation was constructed by bridging a 62-mutant synthetic double-stranded oligonucleotide from a Bpu 1,102 to a Kpn I site. For the double mutations, we used the pSMα His^{408}Ala to introduce the latter mutation. The presence of each mutation was confirmed by dideoxy sequencing.

Transfections and Stable Mutant Cell Lines

CHO-K1 cells were transfected with pSMα (wild-type or mutants), pSMβ, pSMε, pSMδ, and pSV_2neo in the ratio 2:1:1:1:0.1 by the calcium phosphate precipitation technique. Selection and screening of clones was carried out as described previously (Roccamo et al., 1999). Only clonal cell lines that expressed all the ARNs subunits detected by RT-PCR were maintained for experimental use.

Protein Determination

Total protein content was determined by the method of Lowry et al. (1951) using an aliquot of the cell extracts made with 0.1 N NaOH after radioactivity measurements. Bovine serum albumin was used as a standard.

Equilibrium [^{125}I]α-BTX Binding Studies

Surface AChR expression was determined by incubating control and mutant clones (70–80% confluent) with increasing concentrations (1–60 nM) of [^{125}I]α-BTX in cell culture medium for 1 hr at 25°C. At the end of the incubation period, dishes were washed twice with Dulbecco's phosphate-buffered saline (PBS) to remove unbound toxin; cells were removed by scraping and were lysed with 0.1 N NaOH. Radioactivity was measured in a gamma counter with an efficiency of 80%. Nonspecific binding was determined from the radioactivity remaining in the dishes when the cells were first preincubated with 10 μM native α-BTX or 2 mM Carb chloride before the addition of [^{125}I]α-BTX. Nonspecific binding amounted to 10% in control and treated cells. Total AChR was determined after lysis of the cells at 4°C with 1% Triton in 10 mM Tris-HCl buffer, pH 7.4, containing 150 mM NaCl, 5 mM EDTA, and protease inhibitors added to the buffer immediately before use. Briefly, 20–40-μl aliquots of the cell lysates were incubated with toxin (60 nM) in a final volume of 125 μl. The binding reaction was terminated by addition of 100 μl of the incubation reaction to DE-81 paper strips [Whatman; 2 × 2 cm squares for each sample as described by Schmidt and Raftery (1973)]. Alternatively, the total pool of AChR was determined in cells permeabilized with 0.5% saponin as described by Blount and Merlie (1990). The internal pool was calculated as the difference between the total and [^{125}]α-BTX surface binding sites.

Fluorescence Microscopy

To observe the AChR at the plasma membrane, cells were grown on coverslips, labeled with Alexa 488-α-BTX for 1 hr at 4°C, washed with PBS, mounted on glass slides, and observed in vivo. To visualize intracellular AChR, cell-surface AChRs were blocked with excess native α-BTX at 4°C. Cells were then fixed with 4% paraformaldehyde for 15 min and permeabilized for 20 min with 0.1% Triton X-100, followed by labeling with Alexa 594-α-BTX at a final concentration of 1 μg/ml.

To visualize the ER, cells were fixed and permeabilized as described above and incubated with primary antibody (rabbit anticalnexin, 1:1,000) for 1 hr at room temperature in PBS containing 1% bovine serum albumin. Cells were washed with PBS and incubated with secondary fluorophore-conjugated antibody (Alexa Fluor 547 anti-rabbit, 1:1,000) and Alexa Fluor 488-α-BTX in the same buffer for 1 hr at room temperature. Cells were washed three times with PBS before mounting on slides and examined with a Nikon Eclipse E-600 fluorescence microscope. Images were captured by using an SBIG model ST-7 digital charge-coupled device camera (765 × 510 pixels, 9.0 × 9.0 μm pixel size; SBIG, Santa Barbara, CA), thermostatically cooled at −10°C. The ST-7 CCD camera was driven by the CCDOPS software

package (SBING Astronomical Instruments, version 5.02). For all experiments, ×40 (1.0 NA) or ×60 (1.4 NA) oil-immersion objectives were used. Appropriate dichroic and emission filters were employed to avoid crossover of fluorescence emission. Sixteen-bit TIFF images were exported for further off-line analysis. Confocal images were obtained by using a ×60 1.4 N.A. water-immersion objective and a model TCSSP2 Leica confocal microscope and analyzed as described above.

Fluorescence Microscopy Assay of AChR Assembly

To determine the proportion of assembled/unassembled intracellular AChR, we employed a fluorescence microscopy assay based on agonist inhibition of α-BTX binding (Baier and Barrantes, in preparation). Basically, cell-surface AChRs were blocked with native α-BTX, fixed, permeabilized, incubated with 10 mM Carb for 1 hr at room temperature, and subsequently incubated with Alexa 594-α-BTX in the presence of agonist. Control cells were incubated with PBS for the same period. Quantitative measurements of fluorescence intensities (see below) of intracellular AChR label in the presence and absence of agonist provided an estimate of the proportion of unassembled AChR.

Quantitative Fluorescence Microscopy Analysis

Fluorescence images were analyzed with Scion Image 4.0.2 (Scion Corp., Frederick, MD). Fluorescence intensities were measured from 16-bit images by selecting small membrane areas (cell surface AChR) or by delimiting the whole cell (intracellular AChR and unassembled AChR). Fluorescence intensity values were corrected for fluorescence background measured in areas adjacent to the cells. The average fluorescence intensity over distinct areas of the cell surface or whole cells was calculated for randomly chosen cells in phase contrast for each experimental condition. Statistical analysis for each experimental condition was carried out by analyzing the average of three or more different experiments. For illustration purposes, images were processed in Adobe Photoshop 7, scaled with identical parameters, and pseudocolored according to the corresponding emission wavelength.

Density Gradient Centrifugation of Wild-Type and Mutant AChRs

CHO cell lines stably expressing wild-type AChR (CHO-K1/A5) and His^{408}Ala, His^{408}Ala/Arg^{429}Ala, and Arg^{429}Ala mutants were incubated for 1 hr at 4°C with [^{125}I]α-BTX (10–15 nM) in Ham's F-12 medium containing 10% fetal bovine serum, rinsed with PBS to remove unbound toxin, and solubilized in buffered 1% Triton X-100 containing protease inhibitors for 3 hr. Extracts were layered atop 3–20% sucrose gradients in 50 mM Tris-HCl buffer, pH 7.5, containing 1% Triton X-100, 150 mM NaCl and 5 mM EDTA, and centrifuged at 4°C in a Sorvall SW41 rotor for 22 hr at 40,000 rpm. Catalase (11 S), carbonic anhydrase (3.3 S), and [^{125}I]α-BTX (1.7 S) were used as markers.

RESULTS

Expression of α1M4 His^{408} and Arg^{429} AChR Mutants in CHO-K1 Cells

As shown in Figure 1, two positively charged amino acids, Arg^{429} and His^{408}, are located at the extracellular and cytoplasmic-facing ends of the α1M4 TM domain, presumably at the level of the phospholipid head groups. To study the role of these two amino acid residues flanking the two extremes of αM4, a series of single and double mutants was produced and stably coexpressed with wild-type non-α AChR subunits (β, δ, ε) in the heterologous CHO-K1 cell system. His^{408} and Arg^{429} were replaced by an uncharged amino acid (Ala), a residue bearing the opposite charge (Glu), or combinations thereof (His^{408}Ala, Arg^{429}Ala, His^{408}Ala/Arg^{429}Ala, Arg^{429}Glu, and His^{408}Ala/Arg^{429}Glu). We had previously produced CHO-K1/A5, a clone expressing sizeable amounts of wild-type adult (α_2, β, δ, ε) muscle AChR (Roccamo et al., 1999). A first aim of this work was thus accomplished by producing mutant clones of the α1M4 AChR domain in mammalian cell lines. Although this was more elaborate and time consuming, the stability of the cell lines permitted a more thorough analysis with a variety of complementary techniques.

Figure 2 dissects the total and cell-surface [^{125}I]α-BTX binding of the resulting clonal cell lines, normalized to that of the wild-type clonal cell line CHO-K1/A5. Surface [^{125}I]α-BTX binding in these control cells made up 60% ± 1.5% of the total binding. Surface expression diminished to 38% ± 3.5% in the His^{408}Ala mutant, whereas replacement of the positively charged Arg residue in the Arg^{429}Ala clone resulted in values of only 5.2% ± 1.1% cell-surface expression relative to that of control cells. We next tested whether the presence of both mutations in the double mutant would have an additive effect. Paradoxically, the combination of the two in the His^{408}Ala/Arg^{429}Ala double-mutant clone produced a less drastic effect on cell-surface expression levels than that of the individual mutations (20.1% ± 3.9%). Suppression of the two charges at the extremes of α1M4 may thus result in a TM domain having a greater degree of freedom to interact with the adjacent TM segment than the surface-anchor or the cytoplasmic face-anchor single-residue mutants.

Replacement of the cell-surface-exposed Arg^{429} with an amino acid residue of opposite charge resulted in the most drastic impairment of surface expression, with no measurable levels of AChR being detected at the cell surface in either the single (Arg^{429}Glu) or the double (His^{408}Ala/ Arg^{429}Glu) mutants (Fig. 2).

Intracellular AChR levels were measured in parallel by using [^{125}I]α-BTX, as is also illustrated in Figure 2: "total" AChR levels correspond to the sum of cell-surface plus intracellular AChR. The lack of net changes in total AChR (black bars) in His^{408}Ala indicates that the less efficacious targeting of AChR to the cell surface (gray bar) is not a consequence of impaired synthesis of AChR α subunit. The Arg^{429}Ala and His^{408}Ala/Arg^{429}Ala

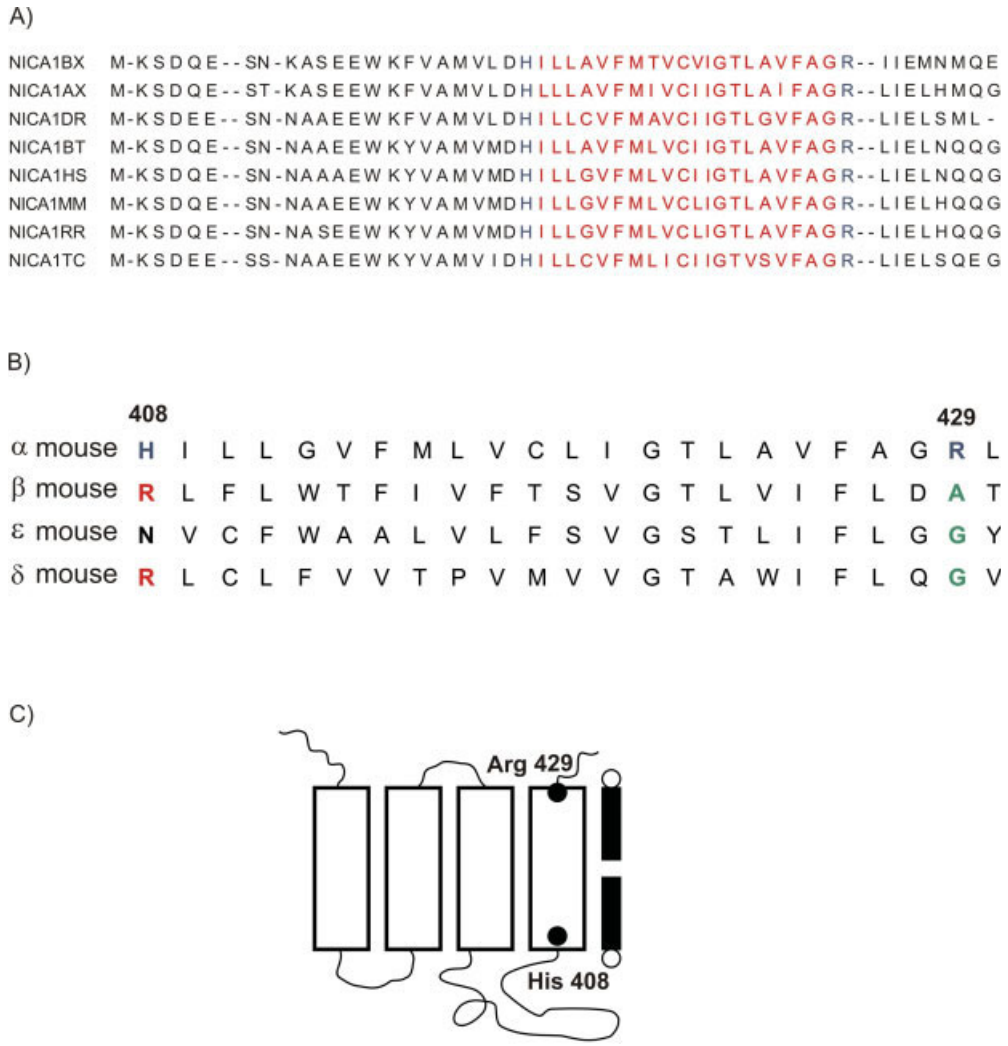

Fig. 1. **A:** Sequence alignment of α1 M4 TM segments from different α subunits across several animal species, showing the 100% conserved His^{408} and Arg^{429} amino acid residues. **B:** The conservation of these two residues is exclusive of α subunits, as illustrated with mouse AChR. The β, ε, and δ subunits depart from this pattern, showing R, N, and R residues at position 408, respectively, and A, G, and G residues at position 429, respectively. **C:** Diagram showing position of the conserved charged amino acid residues flanking each extreme of the αM4 TM segment in close juxtaposition with the charged polar head region of membrane phospholipids. [Color figure can be viewed in the online issue, which is available at www.interscience.wiley.com.]

mutants exhibited less than 20% diminution of intracellular levels: elimination of the charge at the extracellular end of αM4 therefore has a small but consistent effect on retention of the AChR inside the cell (Fig. 2). Reversal of the cell-surface-exposed charge (the Arg^{429} Glu single- and His^{408}Ala/Arg^{429}Glu double mutant) decreased intracellular AChR levels by ∼35% and ∼30%, respectively. Because this type of mutations totally abolished cell-surface expression, the diminution of intracellular levels is clearly a reflection of impaired biosynthesis or, alternatively, defective folding/assembly, followed by elimination of defective subunits.

Intracellular Accumulation of His^{408} and Arg^{429} AChR Mutants

To determine the subcellular distribution of the AChR in wild-type CHO-K1/A5 cells and His^{408} and Arg^{429} mutants, we also studied them by fluorescence microscopy. When cells were stained with Alexa 488-α-BTX for 1 hr at 4°C, a condition leading to cell-surface receptor labeling only (Pediconi et al., 2004; Borroni et al., 2006), control CHO-K1/A5 cells exhibited bright surface fluorescence. Cell-surface Alexa 488-α-BTX fluorescence was about 20% less intense in the His^{408}Ala mutant clonal cell line, and was virtually absent in the

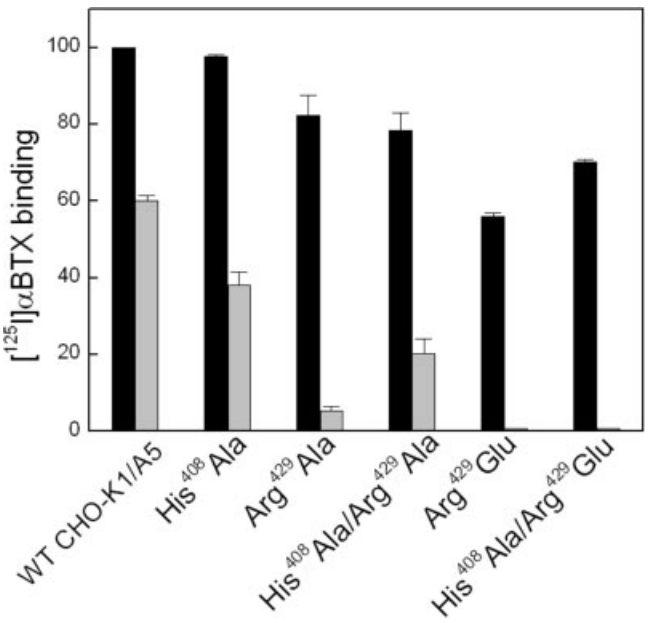

Fig. 2. Total (black bars) and cell-surface (gray bars) α-bungarotoxin binding to the resulting clonal cell lines, normalized to that of the wild-type AChR, the clonal cell line CHO-K1/A5. Intact cells (cell-surface binding) and fixed cells permeabilized with 1% saponin for 5 min (intracellular binding) were incubated with 40 nM [^{125}I]α-BTX for 1 hr at 4°C and lysed as described in Materials and Methods. Total binding is the sum of cell-surface and intracellular AChR. Nonspecific binding was determined in parallel in cells preincubated with 10 μM native α-BTX for 30 min.

His^{408}Ala/Arg^{429}Glu (Fig. 3), Arg^{429}Ala, Arg^{429}Glu, and His^{408}Ala/Arg^{429}Glu mutants (not shown), in agreement with the results of [^{125}I]α-BTX binding (Fig. 2). Another set of wild-type and mutant clones was permeabilized and intracellular AChR labeled with Alexa 594-α-BTX (red). The intracellular fluorescence was observed all over the cytoplasm, with a more accentuated perinuclear distribution in the less severely affected His^{408}Ala mutant, probably reflecting the ability of this mutant to reach the Golgi stage. A more diffuse and faint Alexa 488-α-BTX intracellular fluorescence distribution was apparent in the His^{408}Ala/Arg^{429}Glu mutant (Fig. 3).

Intracellular Accumulation of Severely Defective AChR Occurs at the ER

To ascertain the subcellular localization of the mutant AChRs, confocal fluorescence microscopy studies were carried out on fixed and permeabilized cells stained with Alexa 488-α-BTX and the ER marker calnexin, a constitutive ER protein (Fig. 4). Typical ER staining was apparent for both probes, which exhibited a considerable degree of overlap in the control cells; faint fluorescent staining was observed in mutant AChRs, but the correspondence between Alexa 488-α-BTX and calnexin staining was still noticeable, as is apparent in the example shown (His^{408}Ala/Arg^{429}Glu mutant). This observation, together with the lack of accumulation of Alexa 488-α-BTX fluorescence at the Golgi region in the severely affected mutations (those involving substitution of Arg by Glu residues), suggests that the retention of the αM4-defective AChR mutants occurred at an early stage of the exocytic pathway. In HEK-293 cells, the chaperone calnexin is associated with the isolated α, β, and δ subunits and unassembled, maturely folded nascent α subunit of the AChR, but not with assembled α-δ dimers (Keller et al., 1996).

Intracellular Accumulation of the Severely Mutated AChR Is Associated With Defective AChR Assembly

To test the possibility that AChR traffic was interrupted because of defective oligomerization, we exploited the pharmacological properties of the competitive antagonist α-BTX binding in the presence or absence of the full agonist Carb. We have recently developed a fluorescence microscopy assay based on this strategy (Baier and Barrantes, in preparation). The basis for this assay is that Carb recognizes, binds, and blocks AChR α subunits associated with the ε (or γ in the embryonic AChR) or δ subunits in the form of dimers or trimers with β subunits, but does not bind to unassembled α subunits (Blount and Merlie, 1990). In contrast, α-BTX recognizes both unassembled and assembled α subunits. Therefore, the difference in fluorescence intensity of intracellular AChRs stained in the presence or absence of Carb allows one to determine the percentages of α subunits that are assembled or not. The mean intracellular fluorescence of Alexa-labeled α-BTX fluorescence in the mutant cell lines was calibrated with respect to control CHO-K1/A5 cells in the absence and presence of excess Carb (Fig. 5A). The results are shown in Figure 5B. The fluorescence intensity of unassembled AChR represented only ~20% of the total AChR inside control, CHO-K1/A5 cells. In the case of the His^{408}Ala/Arg^{429}Ala mutant, a drastic change in intracellular Alexa 594-α-BTX fluorescence intensity was apparent. Total intracellular AChR diminished to ~50% of the control value, and, more remarkably, almost all of it corresponded to unassembled AChR (Fig. 5B). Cells expressing the reversed charge (Arg^{429}Glu mutant) stained with Alexa 594-α-BTX in the presence or absence of 10 mM Carb showed a similar profile: intracellular AChR levels diminished, and unassembled forms accounted for most of the intracellular receptor (Fig. 5B).

His^{408}Ala/Arg^{429}Ala and Arg^{429}Ala Double Mutants Do Not Assemble Into Full Pentamers But His^{408} Mutant AChR Does

To dissect further the contribution of the charged flanking amino acid residues in the αM4 segment, a series of experiments was conducted to determine the state of oligomerization of the AChR protein. Cells expressing wild-type and mutant AChR were permeabilized with 0.5% saponin, and AChR was labeled with

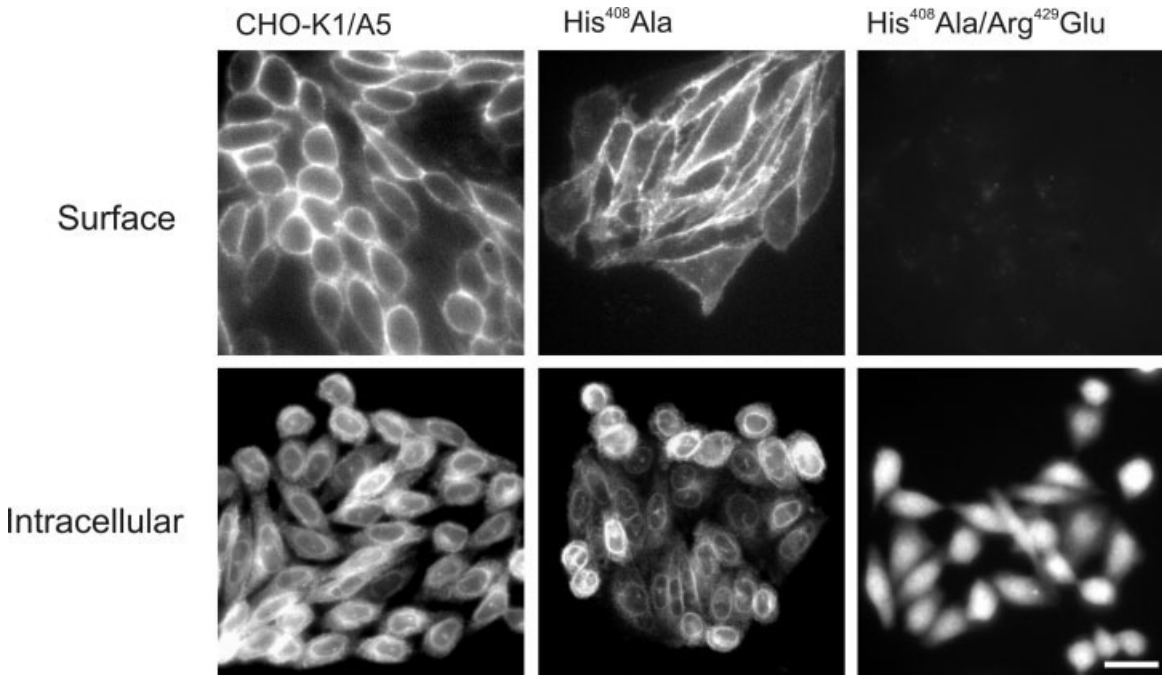

Fig. 3. Cellular distribution of the AChR in wild-type (CHO-K1/A5) and mutant clones by wide-field fluorescence microscopy. The upper panel shows the receptor cell-surface distribution in cells stained with Alexa-488-α-BTX. The lower panel corresponds to the distribution of intracellular AChR in cells fixed, permeabilized, and stained with Alexa-594-α-BTX.

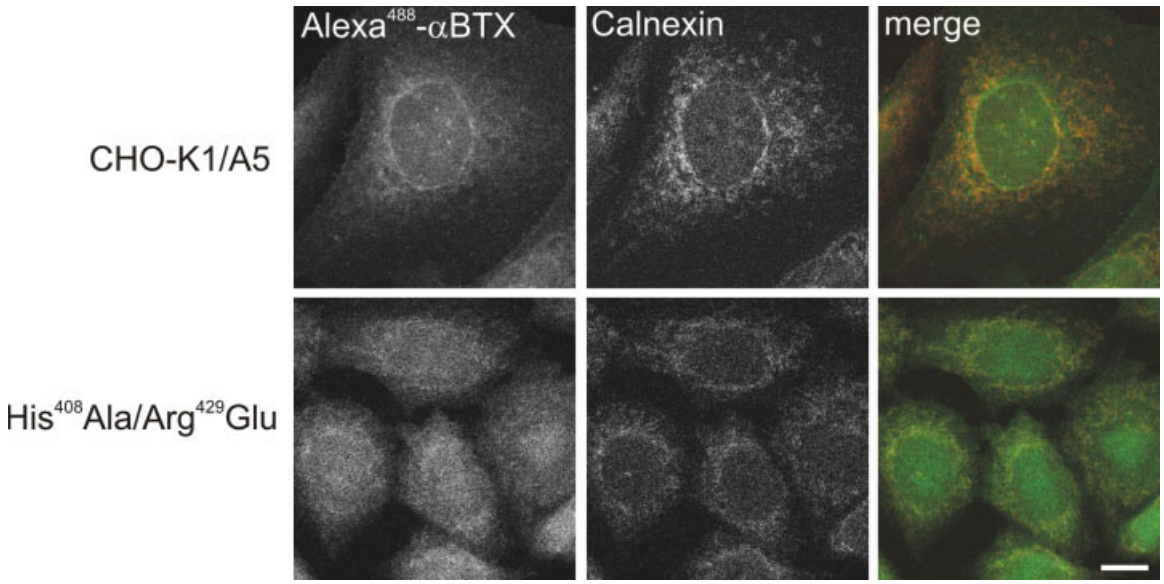

Fig. 4. Confocal fluorescence microscopy of intracellular AChR in fixed and permeabilized cells stained with (green) Alexa 488-α-BTX and an antibody against the ER marker calnexin, a bonafide ER marker, followed by (red) Alexa 597-labeled secondary antibody. Typical ER staining was apparent for both probes, which exhibited a considerable degree of overlap, especially in the perinuclear region of the cell (orange-yellow in the merged image). The fluorescent staining was similar in both the control (CHO-K1/A5 cells) and the mutant clonal cell line expressing $His^{408}Ala/Arg^{429}Glu$ AChR. Scale bar = 10 μm.

[^{125}I]α-BTX. Cells were subsequently solubilized in 1% Triton X-100 and subjected to equilibrium centrifugation in detergent-containing 5–20% sucrose gradients. As shown in Figure 6, wild-type AChR from control CHO-K1/A5 cells migrated predominantly as a single peak of ~9 S. Free α-BTX migrated with a value of ~1.7 S, as previously reported (Kreienkamp et al., 1995). Under similar experimental conditions, *Torpedo marmorata*

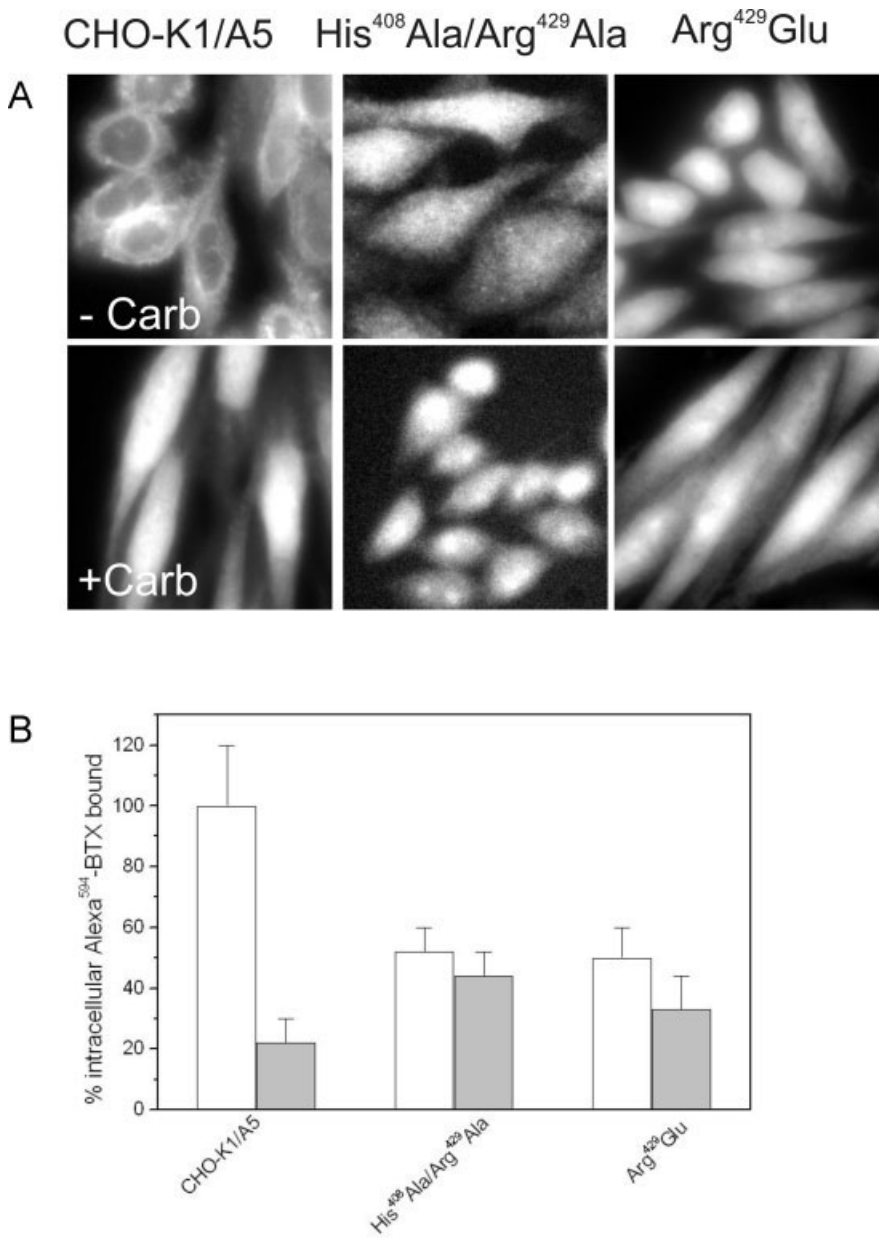

Fig. 5. Unassembled AChR is retained at the ER. **A:** Fluorescence microscopy assay (Baier and Barrantes, unpublished) based on the ability of the agonist Carb to block AChR α subunits associated with the ε or δ subunits in the form of dimers or trimers with β subunits, but not unassembled α subunits (Blount and Merlie, 1990), whereas α-BTX recognizes both unassembled and assembled α subunits. The difference in fluorescence intensity of intracellular AChRs stained in the presence or absence of Carb enables one to determine the percentage of α subunits assembled or not in control and mutant cell lines. The quantitative results are shown in **B**.

AChR has a sedimentation coefficient of 9 S (Barrantes, 1982) and mouse muscle AChR a value of 9.5 S (Kreinkamp et al., 1995). Thus the peak at ~9 S observed in CHO-K1/A5 cells can be attributed to the fully assembled AChR pentamer. In addition to this main peak, wild-type AChR exhibited a minor peak between the 9 S main radioactivity peak and the 3.5 S marker protein carbonic anhydrase. A third, lighter peak, coincident with this marker, was present in the extracts from the CHO-K1/A5 cells and all mutants (Fig. 6). The detergent-solubilized His^{408}Ala mutant displayed the 9 S main peak, albeit with a smaller amplitude relative to that of wild-type AChR (CHO-K1/A5 cells) and those of standard proteins included in the centrifugation run. In contrast, the His^{408}Ala/Arg^{429}Ala mutant and the Arg^{429}Ala mutants did not appear to result in the successful formation of subunit oligomers, exhibiting only the low S value (~3.5) peak, which may be attributed mainly to unassembled [^{125}I]α-BTX-bound α subunit (Fig. 6).

DISCUSSION

The present work examines the functional role of two basic amino acid residues (His^{408} and Arg^{429}) flanking the cytoplasmic- and extracellular-facing ends of αM4, respectively. These charged residues are unique to the α subunit (Fig. 1) and highly invariant among species

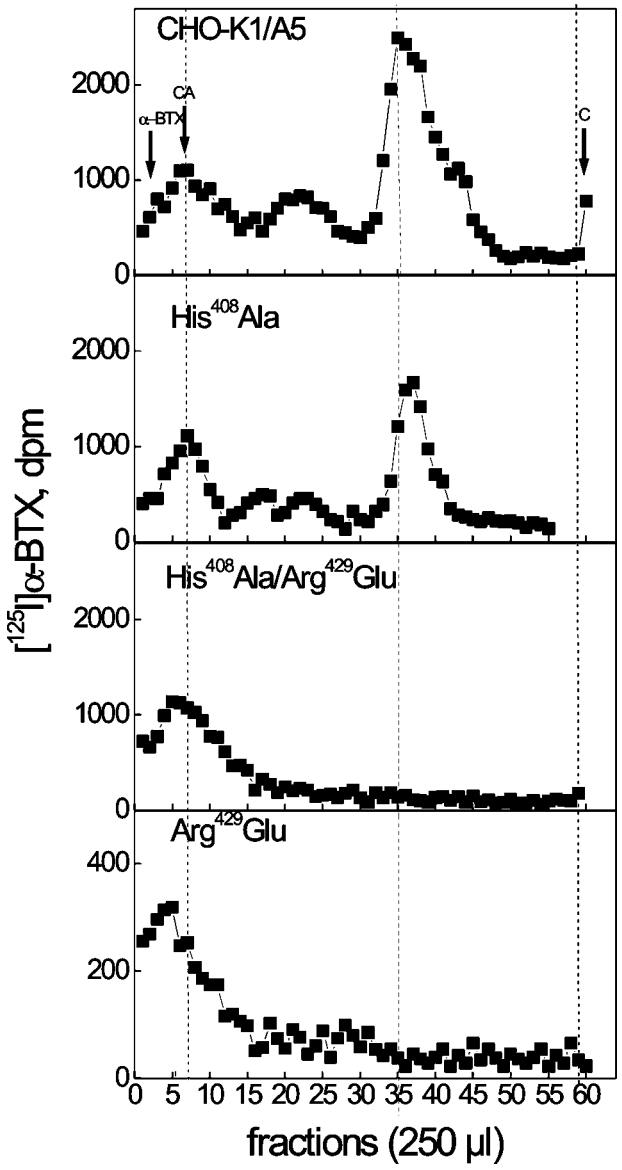

Fig. 6. State of oligomerization of AChR in control and mutant cell lines as determined by equilibrium sucrose density gradient centrifugation. Cells expressing wild-type (CHO-K1 cells) and $His^{408}Ala$, $His^{408}Ala/Arg^{429}Ala$, and $Arg^{429}Ala$ mutant AChR were permeabilized with 0.5% saponin, and AChR was labeled with [^{125}I]α-BTX. Cells were solubilized in 1% Triton X-100, subjected to equilibrium centrifugation in detergent-containing 5–20% sucrose gradients (50 mM Tris-HCl buffer, pH 7.5, containing 1% Triton X-100, 150 mM NaCl, and 5 mM EDTA), and centrifuged for 22 hr at 40,000 rpm at 4°C in a Sorvall SW41 rotor. Free α-BTX migrated with a value of ~1.7 S (Kreienkamp et al., 1995). The equilibrium sedimentation position of catalase (C; 11 S), carbonic anhydrase (CA; 3.3 S) and [^{125}I]α-BTX (1.7 S) is indicated in each case. The relevant [^{125}I]α-BTX peaks are those corresponding to unassembled α subunit (left-most dotted vertical line running across all panels), migrating close to CA, and the fully assembled AChR pentamer (central dotted vertical line).

(Fig. 1), and their replacement by uncharged residues, or amino acid residues of opposite charge, impairs AChR assembly and transport to the plasma membrane. Previous studies showed that mutants $\alpha Arg^{209}Ala$ and $\alpha Arg^{209}Glu$ of *Torpedo californica* AChR exhibit very low levels of cell-surface receptor in comparison with wild-type AChR expressed in *Xenopus* oocytes (Tamamizu et al., 1995). Point mutation of the Arg^{209} (close to the commencement of the M1 TM domain) to Glu or Leu in neuronal α7 AChR leads to impairment of cell-surface expression (Vicente-Agullo et al., 2001).

One of the hypotheses on the mechanisms of membrane protein orientation and assembly holds that positively charged residues in the sequences flanking the TM segments are asymmetrically distributed and that an excess of positively charged residues defines a cytoplasmic domain (von Heijne and Gavel, 1988). Another hypothesis, the "charge difference" rule, proposed for eukaryotic membrane proteins, postulates that the charge differences between the segments flanking TM domains determine orientation, rather than positively charged residues themselves (Hartmann et al., 1989). According to the charge difference rule, negatively and positively charged residues possess an equal topogenic potential (Schülein, 2004). The AChR protein, however, does not fall into any of the canonical categories of multispanning membrane proteins examined in relation to ER targeting (Schülein, 2004), because the topology of its COO^- and NH^+ termini is atypical (both tails of the receptor protein are exposed to the extracellular space).

In addition to receptor-specific factors essential for functional expression of AChRs, host-specific factors have also been implicated. These include posttranslational modifications and chaperones, both of which have been proposed to influence protein folding and assembly of AChRs (Dineley and Patrick, 2000; Drisdel and Green, 2000; Keller at al., 2001; Vicente-Agullo et al., 2001; Schroeder et al., 2003). A recent study on chimeric chick α7/5-HT_3 receptor expression in HEK-293 and PC12 cells (Drisdel and Green, 2000) highlights their importance. Furthermore, α7/5-HT_3 receptors also need to be highly palmitoylated: neither of these features was observed with wild-type α7 AChRs. In contrast, palmitoylation of wild-type α7 AChRs and proper expression did occur in PC12 cells. These posttranslational modifications are unlikely to be involved in the case of the muscle AChR mutants examined here.

Adjacent basic amino acid residues (Arg^{313}-Lys^{314}) in the large M3–M4 of the α-subunit cytoplasmic loop have been shown to be involved in the ER retention of the muscle α1 subunit. This motif is recognized by the COP I complex, and ubiquitination modulates ER to cell-surface trafficking of the AChR in transfected HEK cells (Keller et al., 2001). A sequence signal in the αM1 TM domain of the AChR was found to prevent the surface transport of unassembled AChR subunits. By using alanine-scanning mutagenesis, Wang et al. (2002) identified the signal as a PLFYxxN motif. This signal not only prevents surface targeting of unassembled monomers but

also results in the arrest of partially assembled subunit complexes. Furthermore, the PLFYxxN motif targets unassembled AChR subunits for degradation. The highly conserved Arg^{209} residue, just before the M1 TM domain, is reported to be essential for the transport of assembled neuronal α7 AChRs to the cell surface (Vicente-Agullo et al., 2001), whereas the equivalent position in muscle AChR, when mutated to the opposite charge, exhibits a gain-of-function in terms of ion channel conductance (Tamamizu et al., 1995). Substitution of the α7 cytoplasmic loop with that of α3 or α5 causes differential localization of the AChR in cultured ciliary ganglion neurons (Williams et al., 1998; Temburni et al., 2004). Various chimeras and point mutants composed of rat α7 and alternative regions of the mouse 5-HT_3 receptor have helped in identifying some domains and key amino acids required for the assembly of functional α7 AChR (Dineley and Patrick, 2000). An αM4 Cys^{418}Gly mutant was not expressed at the cell surface of *Xenopus* oocytes (Tamamizu et al., 1999). The αM4 charged motifs identified in the present work are therefore not the only ones involved in AChR assembly and cell-surface targeting, but their unique positions—flanking the two extremes of the purported TM region—are likely to play a key role in these two processes.

REFERENCES

Barrantes FJ. 1982. Oligomeric forms of the membrane-bound acetylcholine receptor disclosed upon extraction of the Mr 43,000 nonreceptor peptide. J Cell Biol 92:60–68.

Barrantes FJ. 2003. Modulation of nicotinic acetylcholine receptor function through the outer and middle rings of transmembrane domains. Curr Opin Drug Discov Devel 6:620–632.

Blanton MP, Cohen JB. 1992. Mapping the lipid-exposed regions in the Torpedo californica nicotinic acetylcholine receptor. Biochemistry 31: 3738–3750.

Blount P, Merlie JP. 1990. Mutational analysis of muscle nicotinic acetylcholine receptor subunit assembly. J Cell Biol 111:2613–2622.

Borroni V, Baier CJ, Lang T, Bonini I, White MW, Garbus I, Barrantes FJ. 2006. Cholesterol depletion activates rapid internalization of diffraction-limited acetylcholine receptor domains at the cell membrane. Molec Membr Bio (in press).

Dineley KT, Patrick JW. 2000. Amino acid determinants of alpha 7 nicotinic acetylcholine receptor surface expression. J Biol Chem 275:1385–1397.

Drisdel RC, Green WN. 2000. Neuronal alpha-bungarotoxin receptors are alpha 7 subunit homomers. J Neurosci 20:133–139.

Gu Y, Camacho P, Gardner P, Hall ZW. 1991. Identification of two amino acid residues in the epsilon subunit that promote mammalian muscle acetylcholine receptor assembly in COS cells. Neuron 6:879–687.

Hartmann E, Rapoport TA, Lodish HF. 1989. Predicting the orientation of eukaryotic membrane-spanning proteins. Proc Natl Acad Sci U S A 86:5786–5790.

Karlin A. 2002. Emerging structure of the nicotinic acetylcholine receptors. Nat Rev Neurosci 3:102–114.

Keller SH, Lindstrom JE, Taylor P. 1996. Involvement of the chaperone protein calnexin and the acetylcholine receptor beta-subunit in the assembly and cell surface expression of the receptor. J Biol Chem 271: 22871–22877.

Keller SH, Lindstrom J, Ellisman M, Taylor P. 2001. Adjacent basic amino residues recognized by the COP I complex and ubiquitination govern endoplasmic reticulum to cell surface trafficking of the nicotinic acetylcholine receptor. J Biol Chem 276:18384–18391.

Kreienkamp H-J, Maeda RK, Sine SM, Taylor P. 1995. Intersubunit contacts governing assembly of the mammalian nicotinic acetylcholine receptor. Neuron 14:635–644.

Lowry OH, Rosebrough NJ, Farr AL, Randall RJ. 1951. Protein measurement with the Folin phenol reagent. J Biol Chem 193:265–275.

Merlie JP, Lindstrom J. 1983. Assembly in vivo of mouse muscle acetylcholine receptor identification of an α subunits species that may be an assembly intermediate. Cell 34:747–757.

Pediconi MF, Gallegos CE, De Los Santos EB, Barrantes FJ. 2004 Metabolic cholesterol depletion hinders cell-surface trafficking of the nicotinic acetylcholine receptor. Neuroscience 128:239–249.

Roccamo AM, Pediconi MF, Aztiria E, Zanello L, Wolstenholme A, Barrantes FJ. 1999. Cells defective in sphingolipids biosynthesis express low amounts of muscle nicotinic acetylcholine receptor. Eur J Neurosci 11:1615–1623.

Schmidt J, Raftery MA. 1973. Purification of acetylcholine receptors from Torpedo californica electroplax by affinity chromatography. Biochemistry 12:852–855.

Schroeder KM, Wu J, Zhao L, Lukas RJ. 2003. Regulation by cycloheximide and lowered temperature of cell-surface alpha7-nicotinic acetylcholine receptor expression on transfected SH-EP1 cells. J Neurochem 85:581–591.

Schülein R. 2004. The early stages of the intracellular transport of membrane proteins: clinical and pharmacological implications Rev Physiol Biochem Pharmacol 151:45–91.

Smith MM, Lindstrom J, Merlie J. 1987. Formation of the α bungarotoxin binding site and assembly of the acetylcholine receptor subunits occur in the endoplamasmic reticulum. J Biol Chem 262:4367–4376.

Tamamizu S, Lee Y, Hung B, McNamee MG, Lasalde-Dominicci JA. 1999. Alteration in ion channel function of mouse nicotinic acetylcholine receptor by mutations in the M4 transmembrane domain. J Membr Biol 170:157–164.

Tamamizu S, Todd AP, McNamee MG. 1995. Mutations in the M1 region of the nicotinic acetylcholine receptor alter the sensitivity to inhibition by quinacrine. Cell Mol Neurobiol 15:427–438.

Temburni MK, Rosenberg MM, Pathak N, McConnell R, Jacob MH. 2004. Neuronal nicotinic synapse assembly requires the adenomatus polyposis coli tumor suppressor protein. J Neurosci 24:6776–6784.

Vicente-Agullo F, Rovira JC, Sala S, Sala F, Rodriguez-Ferrer C, Campos-Caro A, Criado M, Ballesta JJ. 2001. Multiple roles of the conserved key residue arginine 209 in neuronal nicotinic receptors. Biochemistry 27:8300–8306.

von Heijne G. 1989. Control of topology and mode of assembly of a polytopic membrane protein by positively charged residues. Nature 341:456–458.

von Heijne G, Gavel Y. 1988. Topogenic signals in integral membrane proteins. Eur J Biochem 174:671–678.

Wanamaker CP, Christianson JC, Green WN. 2003. Regulation of nicotinic acetylcholine receptor assembly. Ann N Y Acad Sci 998:66–80.

Wang JM, Zhang L, Yao Y, Viroonchatapan N, Rothe E, Wang ZZ. 2002. A transmembrane motif governs the surface trafficking of nicotinic acetylcholine receptors. Nat Neurosci 5:963–970.

Williams J, Bates S, Griebel ML, Lange B, Mancias P, Pihoker CM, Dykman R. 1998. Does short-term anti-epileptic drug treatment in children result in cognitive or behavioral changes? Epilepsia 39:1064–1069.